J. Fluid Mech. (2001), *vol.* 445, *pp.* 263–283.
DOI: 10.1017/S0022112001005572 Printed in the United Kingdom

Viscous potential flow analysis of Kelvin–Helmholtz instability in a channel

By T. FUNADA[1] AND D. D. JOSEPH[2]

[1]Department of Digital Engineering, Numazu College of Technology, Ooka 3600, Numazu, Shizuoka, Japan

[2]Department of Aerospace Engineering and Mechanics, University of Minnesota, Minneapolis, MN 55455, USA

(Received 6 November 2000 and in revised form 2 May 2001)

We study the stability of stratified gas–liquid flow in a horizontal rectangular channel using viscous potential flow. The analysis leads to an explicit dispersion relation in which the effects of surface tension and viscosity on the normal stress are not neglected but the effect of shear stresses is. Formulas for the growth rates, wave speeds and neutral stability curve are given in general and applied to experiments in air–water flows. The effects of surface tension are always important and determine the stability limits for the cases in which the volume fraction of gas is not too small. The stability criterion for viscous potential flow is expressed by a critical value of the relative velocity. The maximum critical value is when the viscosity ratio is equal to the density ratio; surprisingly the neutral curve for this viscous fluid is the same as the neutral curve for inviscid fluids. The maximum critical value of the velocity of all viscous fluids is given by that for inviscid fluid. For air at 20 °C and liquids with density $\rho = 1\,\mathrm{g\,cm^{-3}}$ the liquid viscosity for the critical conditions is 15 cP: the critical velocity for liquids with viscosities larger than 15 cP is only slightly smaller but the critical velocity for liquids with viscosities smaller than 15 cP, like water, can be much lower. The viscosity of the liquid has a strong effect on the growth rate. The viscous potential flow theory fits the experimental data for air and water well when the gas fraction is greater than about 70%.

1. Introduction

It is well known that the Navier–Stokes equations are satisfied by potential flow; the viscous term is identically zero when the vorticity is zero but the viscous stresses are not zero (Joseph & Liao 1994). It is not possible to satisfy the no-slip condition at a solid boundary or the continuity of the tangential component of velocity and shear stress at a fluid–fluid boundary when the velocity is given by a potential. The viscous stresses enter the viscous potential flow analysis of free surface problems through the normal stress balance (2.9) at the interface. Viscous potential flow analysis gives good approximations to fully viscous flows in cases where the shear from the gas flow is negligible; the Rayleigh–Plesset bubble is a potential flow which satisfies the Navier–Stokes equations and all the interface conditions. Joseph, Belanger & Beavers (1999) constructed a viscous potential flow analysis of the Rayleigh–Taylor instability which is almost indistinguishable from the exact fully viscous analysis.

The success of viscous potential flow in the analysis of Rayleigh–Taylor instability has motivated the analysis of Kelvin–Helmholtz (KH) theory given here. It is well

known that the instability that arises when surface tension and viscosity are neglected is catastrophic: short waves with wavelengths $\lambda = 2\pi/k$ amplify without control like e^{kt}. The instability grows exponentially as the wavenumber $k \to \infty$ no matter how small time t. This kind of catastrophic instability is called Hadamard instability (Joseph & Saut 1990). In the case of inviscid fluids this instability is regularized by surface tension which stabilizes the short waves; surface tension is very important. The question is whether viscosity, without surface tension, would regularize the Hadamard instability of a vortex sheet on an unbounded domain. Unlike surface tension, viscosity will not cause the small waves to decay; they still grow but their growth is limited and the growth rate $\mathrm{Re}[\sigma(k)]$ does not go to infinity with k as in Hadamard instability. The positive growth rate is given by

$$\mathrm{Re}[\sigma_+] = \frac{\rho_a\mu_l^2 + \rho_l\mu_a^2}{2(\mu_l + \mu_a)^3}(U_a - U_l)^2, \quad k \to \infty,$$

where ρ, μ, U are respectively density, viscosity, velocity.

The present paper gives a detailed report on the viscous potential flow analysis of KH instability in a rectangular duct together with a comparison of theory and experiment in the case of air–water flow. As we have already mentioned, potential flow requires that we neglect the no-slip condition at solid surfaces. In a rectangular channel the top and bottom walls are perpendicular to gravity; the bottom wall is under the liquid and parallel to the undisturbed uniform stream; the top wall contacts gas only. The sidewalls are totally inactive; there is no motion perpendicular to the sidewalls unless it is created initially and since the two fluids slip at the walls all the conditions required in the analysis of three dimensions can be satisfied by flow in two dimensions, which is analysed here.

The viscosity in viscous potential flow enters the normal stress balance rather than the tangential stress balance. Air over liquid induces small viscous stresses that may be confined to the boundary layer and may be less and less important as the viscosity of the liquid increases. At a flat, free surface $z = 0$ with velocity components (u, w) corresponding to (x, z) the shear stress is given by

$$\mu\left(\frac{\partial u}{\partial z} + \frac{\partial w}{\partial x}\right)$$

and the normal stress is

$$2\mu\frac{\partial w}{\partial z}.$$

The normal stress is an extensional rather than a shear stress and it is activated by waves on the liquid; the waves are induced more by pressure than by shear. For this reason, we could argue that the neglect of shear could be justified in wave motions in which the viscous resistance to wave motion is not negligible; this is the situation which may be approximated well by viscous potential flow.

2. Formulation of the problem

A channel of rectangular cross-section with height H and width W and of length L is set horizontally, in which a gas layer is over a liquid layer (see figure 1): the two-layer Newtonian incompressible fluids are immiscible. The undisturbed interface is taken at $z = 0$ on the z-axis of Cartesian coordinates (x, y, z). We denote velocity by (u, w), pressure p, density ρ, viscosity μ and acceleration due to gravity $(0, -g)$; the y component is ignored herein.

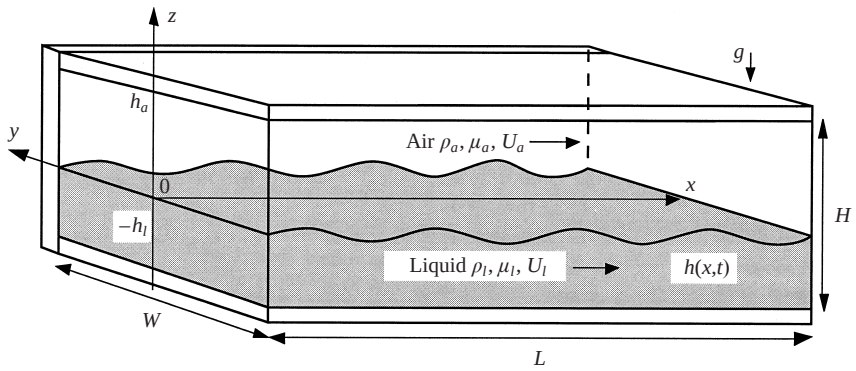

FIGURE 1. Kelvin–Helmholtz instability due to a discontinuity of velocity of air above liquid in a rectangular channel. The no-slip condition is not enforced in viscous potential flow so that the two-dimensional solution satisfies the sidewall boundary conditions.

In the undisturbed state, the gas (air) with a uniform flow $(U_a, 0)$ is in $0 < z < h_a$, and the liquid with a uniform flow $(U_l, 0)$ is in $-h_l < z < 0$ $(H = h_l + h_a)$; the pressure has an equilibrium distribution due to the gravity. We consider Kelvin–Helmholtz instability of small disturbances to the undisturbed state.

The prescription of a discontinuity in velocity across $z = 0$ is not compatible with the no-slip condition of Navier–Stokes viscous fluid mechanics. The discontinuous prescription of data in the study of Kelvin–Helmholtz instability is a viscous potential flow solution of the Navier–Stokes equation in which no-slip conditions at the walls and no slip and continuity of shear stress across the gas–liquid interface are neglected. Usually the analysis of Kelvin–Helmholtz instability is done using potential flow for an inviscid fluid but this procedure leaves out certain effects of viscosity which can be included with complete rigour. This kind of analysis using viscous potential flow is carried out here. An exact study of, say, air over water requires the inclusion of all of the effects of viscosity, and even the prescription of a basic flow is much more complicated. Problems of superposed viscous fluids have been considered, for example, in the monograph on two-fluid mechanics by Joseph & Renardy (1991) and more recently in the paper and references therein of Charru & Hinch (2000).

2.1. *Viscous potential flow analysis*

We have already noted that if the fluids are allowed to slip at the walls, then the two-dimensional solution will satisfy the three-dimensional equations and we may reduce the analysis to flow between parallel plates. We found by computing that three-dimensional disturbances are more stable than two-dimensional ones. We now consider two-dimensional disturbances, for which the velocity potential $\phi \equiv \phi(x, z, t)$ gives $(u, w) = \nabla\phi$.

The potential is subject to the equation of continuity:

$$\frac{\partial u}{\partial x} + \frac{\partial w}{\partial z} = 0 \rightarrow \frac{\partial^2 \phi}{\partial x^2} + \frac{\partial^2 \phi}{\partial z^2} = 0; \tag{2.1}$$

thus the potentials for the respective fluids are given by

$$\frac{\partial^2 \phi_a}{\partial x^2} + \frac{\partial^2 \phi_a}{\partial z^2} = 0 \quad \text{in} \quad 0 < z < h_a, \tag{2.2}$$

$$\frac{\partial^2 \phi_l}{\partial x^2} + \frac{\partial^2 \phi_l}{\partial z^2} = 0 \quad \text{in} \quad -h_l < z < 0. \tag{2.3}$$

Boundary conditions at the interface (at $z = h$, where $h \equiv h(x,t)$ is the interface elevation) are given by

$$\frac{\partial h}{\partial t} + U_a \frac{\partial h}{\partial x} = w_a, \quad \frac{\partial h}{\partial t} + U_l \frac{\partial h}{\partial x} = w_l, \tag{2.4a,b}$$

and the conditions on the walls are given by

$$w_a = 0 \quad \text{at} \quad z = h_a, \tag{2.5}$$

$$w_l = 0 \quad \text{at} \quad z = -h_l. \tag{2.6}$$

The potential ϕ_a that satisfies (2.2) and (2.5) for the air and the potential ϕ_l that satisfies (2.3) and (2.6) for the liquid are given, respectively, by

$$\phi_a = A_a \cosh[k(z - h_a)] \exp(\sigma t + \mathrm{i}kx) + \text{c.c.}, \tag{2.7a}$$

$$\phi_l = A_l \cosh[k(z + h_l)] \exp(\sigma t + \mathrm{i}kx) + \text{c.c.}, \tag{2.7b}$$

and the interface elevation may be given by

$$h = A_0 \exp(\sigma t + \mathrm{i}kx) + \text{c.c.}, \tag{2.7c}$$

where A_a, A_l and A_0 denote the complex amplitudes, and c.c. stands for the complex conjugate of the preceding expression; σ is the complex growth rate and $k > 0$ denotes the wavenumber; $\mathrm{i} = \sqrt{-1}$. From the kinematic conditions (2.4a, b), we have the following equations for the complex amplitudes:

$$(\sigma + \mathrm{i}kU_a)A_0 = -kA_a \sinh(kh_a), \tag{2.8a}$$

$$(\sigma + \mathrm{i}kU_l)A_0 = kA_l \sinh(kh_l). \tag{2.8b}$$

The other boundary condition is the normal stress balance (with the normal viscous stress) at the interface:

$$-p_a + 2\mu_a \frac{\partial w_a}{\partial z} + \rho_a g h - \left(-p_l + 2\mu_l \frac{\partial w_l}{\partial z} + \rho_l g h \right) = -\gamma \frac{\partial^2 h}{\partial x^2}, \tag{2.9}$$

in which γ denotes the surface tension. Noting that the pressure is solely subject to the Laplace equation derived from the equation of motion for small disturbances, the pressure terms in (2.9) may be eliminated using the equations of motion in which the viscous terms vanish identically when $\boldsymbol{u} = \nabla\phi$; $\mu\nabla^2\boldsymbol{u} = \mu\nabla(\nabla^2\phi) \equiv 0$. Thus p_a may be written, from the equation of motion without the viscous term, as

$$\rho_a \left(\frac{\partial u_a}{\partial t} + U_a \frac{\partial u_a}{\partial x} \right) = -\frac{\partial p_a}{\partial x}, \tag{2.10a}$$

and with the aid of the equation of continuity, we have the expression for p_a:

$$\rho_a \left(\frac{\partial^2 w_a}{\partial t \partial z} + U_a \frac{\partial^2 w_a}{\partial x \partial z} \right) = \frac{\partial^2 p_a}{\partial x^2}; \tag{2.10b}$$

the pressure p_l may be written as

$$\rho_l \left(\frac{\partial^2 w_l}{\partial t \partial z} + U_l \frac{\partial^2 w_l}{\partial x \partial z} \right) = \frac{\partial^2 p_l}{\partial x^2}. \tag{2.11}$$

Thus the normal stress balance is now written as

$$-\rho_a\left(\frac{\partial^2 w_a}{\partial t\partial z}+U_a\frac{\partial^2 w_a}{\partial x\partial z}\right)+2\mu_a\frac{\partial^3 w_a}{\partial x^2\partial z}+\rho_l\left(\frac{\partial^2 w_l}{\partial t\partial z}+U_l\frac{\partial^2 w_l}{\partial x\partial z}\right)$$
$$-2\mu_l\frac{\partial^3 w_l}{\partial x^2\partial z}-(\rho_l-\rho_a)g\frac{\partial^2 h}{\partial x^2}=-\gamma\frac{\partial^4 h}{\partial x^4}, \quad (2.12)$$

hence we have the equation for σ, using (2.7) and (2.8):

$$[\rho_a(\sigma+\mathrm{i}kU_a)^2+2\mu_a k^2(\sigma+\mathrm{i}kU_a)]\coth(kh_a)$$
$$+[\rho_l(\sigma+\mathrm{i}kU_l)^2+2\mu_l k^2(\sigma+\mathrm{i}kU_l)]\coth(kh_l)+(\rho_l-\rho_a)gk+\gamma k^3=0. \quad (2.13)$$

2.2. *Dispersion relation*

From (2.13) the dispersion relation is given as

$$A\sigma^2+2B\sigma+C=0, \quad (2.14)$$

where the coefficients A, B and C are defined as

$$A=\rho_l\coth(kh_l)+\rho_a\coth(kh_a), \quad (2.15a)$$

$$B=\mathrm{i}k[\rho_l U_l\coth(kh_l)+\rho_a U_a\coth(kh_a)]$$
$$+k^2[\mu_l\coth(kh_l)+\mu_a\coth(kh_a)]=B_R+\mathrm{i}B_I, \quad (2.15b)$$

$$C=(\rho_l-\rho_a)gk-k^2[\rho_l U_l^2\coth(kh_l)+\rho_a U_a^2\coth(kh_a)]+\gamma k^3$$
$$+2\mathrm{i}k^3[\mu_l U_l\coth(kh_l)+\mu_a U_a\coth(kh_a)]=C_R+\mathrm{i}C_I. \quad (2.15c)$$

The solution σ may be expressed as

$$\sigma=-\frac{B}{A}\pm\sqrt{\frac{B^2}{A^2}-\frac{C}{A}}\to\sigma_R+\mathrm{i}\sigma_I=-\frac{B_R+\mathrm{i}B_I}{A}\pm\frac{\sqrt{D}}{A}, \quad (2.16)$$

where D is given by

$$D=D_R+\mathrm{i}D_I=(B_R+\mathrm{i}B_I)^2-A(C_R+\mathrm{i}C_I), \quad (2.17a)$$

$$D_R=\rho_l\rho_a(U_a-U_l)^2k^2\coth(kh_l)\coth(kh_a)k^4[\mu_l\coth(kh_l)+\mu_a\coth(kh_a)]^2$$
$$-[\rho_l\coth(kh_l)+\rho_a\coth(kh_a)][(\rho_l-\rho_a)gk+\gamma k^3], \quad (2.17b)$$

$$D_I=2k^3(\rho_a\mu_l-\rho_l\mu_a)(U_a-U_l)\coth(kh_l)\coth(kh_a). \quad (2.17c)$$

When $\rho_a\mu_l=\rho_l\mu_a$ for which $D_I=0$, and if $D_R\geqslant 0$, we have

$$\sigma_R=\frac{-B_R\pm\sqrt{D_R}}{A}, \quad \sigma_I=-\frac{B_I}{A}. \quad (2.18a,b)$$

This is a typical case where the real and imaginary parts of σ can be expressed most clearly.

If the top and bottom are far away, $h_l\to\infty, h_a\to\infty$, then (2.14) gives rise to

$$\sigma=-\frac{\mathrm{i}k(\rho_a U_a+\rho_l U_l)+k^2(\mu_a+\mu_l)}{(\rho_a+\rho_l)}$$
$$\pm\left[\frac{\rho_a\rho_l k^2(U_a-U_l)^2}{(\rho_a+\rho_l)^2}-\frac{(\rho_l-\rho_a)gk+\gamma k^3}{(\rho_a+\rho_l)}+\frac{k^4(\mu_a+\mu_l)^2}{(\rho_a+\rho_l)^2}\right.$$
$$\left.+2\mathrm{i}k^3\frac{(\rho_a\mu_l-\rho_l\mu_a)(U_a-U_l)}{(\rho_a+\rho_l)^2}\right]^{1/2},$$

which is reduced, for a particular case that $\rho_a\mu_l = \rho_l\mu_a$, to

$$\sigma_R = -\frac{k^2(\mu_a+\mu_l)}{(\rho_a+\rho_l)} \pm \left[\frac{\rho_a\rho_l k^2(U_a-U_l)^2}{(\rho_a+\rho_l)^2} - \frac{(\rho_l-\rho_a)gk+\gamma k^3}{(\rho_a+\rho_l)} + \frac{k^4(\mu_a+\mu_l)^2}{(\rho_a+\rho_l)^2}\right]^{1/2}, \tag{2.19a}$$

$$\sigma_I = -\frac{k(\rho_a U_a + \rho_l U_l)}{(\rho_a+\rho_l)}. \tag{2.19b}$$

Here, it is easy to find that $\sigma_R = 0$ gives a relation independent of viscosity. In other words, the relation holds even for inviscid fluids; this is helpful for the problem to be considered herein.

2.3. *Growth rates and wave speeds*

In terms of $\sigma = \sigma_R + \mathrm{i}\sigma_I$, (2.14) is also written, for the real and imaginary parts, as

$$A(\sigma_R^2 - \sigma_I^2) + 2(B_R\sigma_R - B_I\sigma_I) + C_R = 0, \quad \sigma_I = -\frac{2B_I\sigma_R + C_I}{2(A\sigma_R + B_R)}. \tag{2.20a,b}$$

Eliminating σ_I from the above, we have a quartic equation for σ_R:

$$a_4\sigma_R^4 + a_3\sigma_R^3 + a_2\sigma_R^2 + a_1\sigma_R + a_0 = 0, \tag{2.21}$$

where the coefficients are given as

$$a_4 = A^3, \quad a_3 = 4A^2B_R, \quad a_2 = 5AB_R^2 + AB_I^2 + A^2C_R, \tag{2.22a,b,c}$$

$$a_1 = 2B_R^3 + 2B_RB_I^2 + 2AB_RC_R, \quad a_0 = -\tfrac{1}{4}AC_I^2 + B_RB_IC_I + B_R^2C_R. \tag{2.22d,e}$$

The quartic equation (2.21) can be solved analytically. Neutral states for which $\sigma_R = 0$ are described in terms of the solution to the equation $a_0 = 0$. The peak value (the maximum growth rate) σ_m and the corresponding wavenumber k_m are obtained by solving (2.21). It is usually true, but unproven, that $\lambda_m = 2\pi/k_m$ will be the length of unstable waves observed in experiments.

The complex values of σ are frequently expressed in terms of a complex frequency ω with

$$\sigma_R + \mathrm{i}\sigma_I = \sigma = -\mathrm{i}\omega = -\mathrm{i}\omega_R + \omega_I. \tag{2.23}$$

Hence

$$\sigma_R = \omega_I, \quad \sigma_I = -\omega_R. \tag{2.24}$$

The wave speed for the mode with wavenumber k is

$$\tilde{C}_R = \omega_R/k = -\sigma_I/k. \tag{2.25}$$

The set of wavenumbers for which unstable flows are stable is also of interest. The wavelengths corresponding to these wavenumbers will not appear in the spectrum. Cut-off wavenumbers k_C separate the unstable and stable parts of the spectrum.

2.4. *Neutral curves*

Neutral curves define values of the parameters for which $\sigma_R(k) = 0$. These curves may be obtained by putting $a_0 = 0$:

$$-\frac{\rho_l\mu_a^2\coth(kh_l)\coth^2(kh_a) + \rho_a\mu_l^2\coth^2(kh_l)\coth(kh_a)}{[\mu_l\coth(kh_l) + \mu_a\coth(kh_a)]^2}kV^2 + (\rho_l-\rho_a)g + \gamma k^2 = 0, \tag{2.26}$$

where the relative velocity V is defined by $V \equiv U_a - U_l$. This equation may be solved for V^2 where

$$V^2(k) = \frac{[\mu_l \coth(kh_l) + \mu_a \coth(kh_a)]^2}{\rho_l \mu_a^2 \coth(kh_l)\coth^2(kh_a) + \rho_a \mu_l^2 \coth^2(kh_l)\coth(kh_a)} \times \frac{1}{k}[(\rho_l - \rho_a)g + \gamma k^2]. \quad (2.27)$$

The lowest point on the neutral curve $V^2(k)$ is

$$V_c^2 = \min_{k \geqslant 0} V^2(k) \equiv V^2(k_c), \quad (2.28)$$

where $\lambda_c = 2\pi/k_c$ is the wavelength that makes V^2 minimum. The flow is unstable when

$$V^2 = (-V)^2 > V_c^2. \quad (2.29)$$

This criterion is symmetric with respect to V and $-V$, depending only on the absolute value of the difference. This feature stems from Galilean invariance: the flow seen by an observer moving with the gas is the same as the one seen by an observer moving with the liquid.

By recalling the results obtained by computing, it is interesting to note here that the three-dimensional disturbances in the sense of the viscous potential flow lead to the relative velocity V_{3D}, which can be expressed in terms of (2.27) as

$$V_{3D}^2 \equiv \frac{(\boldsymbol{k} \cdot \boldsymbol{U}_a - \boldsymbol{k} \cdot \boldsymbol{U}_l)^2}{k_x^2} = \frac{k^2}{k_x^2} V^2(k), \quad (2.30)$$

only if we regard the three-dimensional-wavenumber vector $\boldsymbol{k} = (k_x, k_y)$ as

$$k = \sqrt{k_x^2 + k_y^2}, \quad k_y = 0, \pm\frac{\pi}{W}, \pm\frac{2\pi}{W}, \cdots. \quad (2.31a, b)$$

It is evident in (2.30) that V_{3D}^2 is larger than $V^2(k)$ if $k_y \neq 0$; the most dangerous three-dimensional disturbance is two-dimensional with $k_y = 0$.

3. KH instability of inviscid fluid

For inviscid fluids ($\mu_a = \mu_l = 0$), we have $B_R = 0$ and $C_I = 0$; thus $a_3 = a_1 = a_0 = 0$ and (2.21) reduces to

$$a_4 \sigma_R^4 + a_2 \sigma_R^2 = 0; \quad (3.1)$$

thus we have

$$a_4 \sigma_R^2 + a_2 = 0, \quad (3.2)$$

and

$$\sigma_I = -\frac{B_I}{A} = -\frac{k[\rho_l U_l \coth(kh_l) + \rho_a U_a \coth(kh_a)]}{\rho_l \coth(kh_l) + \rho_a \coth(kh_a)}. \quad (3.3)$$

It should be noted here that the neutral curve was given by the equation $a_0 = 0$ in the viscous potential analysis ((2.26) and (2.27)), whereas the neutral curve in this K-H instability is given by the equation $a_2 = 0$. It is also noted that σ_I is the same as in (2.18*b*), though σ_R may be different, in general, from (2.18*a*). But the equation $\sigma_R = 0$ in (3.2) is the same as $\sigma_R = 0$ in (2.18*a*), for the case of $\rho_a \mu_l = \rho_l \mu_a$.

From (3.2) with $a_2 < 0$, the growth rate σ_R is expressed as

$$\sigma_R = \pm \frac{\sqrt{\rho_l \rho_a k^2 \coth(kh_l)\coth(kh_a)V^2 - [\rho_l \coth(kh_l) + \rho_a \coth(kh_a)][(\rho_l - \rho_a)gk + \gamma k^3]}}{\rho_l \coth(kh_l) + \rho_a \coth(kh_a)}. \tag{3.4}$$

At the neutral state $\sigma_R = 0$ for which $a_2 = 0$, we have

$$\frac{\rho_l \rho_a k \coth(kh_l)\coth(kh_a)}{\rho_l \coth(kh_l) + \rho_a \coth(kh_a)} V^2 - [(\rho_l - \rho_a)g + \gamma k^2] = 0. \tag{3.5}$$

Instability arises if

$$V^2 > \left[\frac{\tanh(kh_l)}{\rho_l} + \frac{\tanh(kh_a)}{\rho_a}\right] \frac{1}{k} \left[(\rho_l - \rho_a)\, g + \gamma k^2\right] \equiv V_i^2(k). \tag{3.6}$$

In the stable case for which $a_2 > 0$, the wave velocity $\tilde{C}_R$ is given by

$$-k\tilde{C}_R = \sigma_I = -\frac{B_I}{A} \pm \sqrt{\frac{B_I^2}{A^2} + \frac{C_R}{A}}. \tag{3.7}$$

4. Dimensionless form of the dispersion equation

The dimensionless variables are designated with a hat and are

$$\hat{k} = kH, \quad \hat{h}_a = \frac{h_a}{H} \equiv \alpha, \quad \hat{h}_l = \frac{h_l}{H} = 1 - \hat{h}_a, \quad \hat{\rho} = \frac{\rho_a}{\rho_l}, \quad \hat{\mu} = \frac{\mu_a}{\mu_l}, \quad \hat{\gamma} = \frac{\gamma}{\rho_l g H^2},$$

$$\hat{U}_a = \frac{U_a}{Q}, \quad \hat{U}_l = \frac{U_l}{Q}, \quad \hat{V} = \hat{U}_a - \hat{U}_l, \quad \hat{\sigma} = \frac{\sigma H}{Q}, \quad \theta = \frac{\mu_l}{\rho_l H Q},$$

where

$$Q = \left[\frac{(1-\hat{\rho})gH}{\hat{\rho}}\right]^{1/2}.$$

The dimensionless form of (2.14) is given by

$$\begin{aligned}
&[\coth(\hat{k}\hat{h}_l) + \hat{\rho}\coth(\hat{k}\hat{h}_a)]\hat{\sigma}^2 \\
&\quad + 2\hat{\sigma}\{i\hat{k}[\hat{U}_l \coth(\hat{k}\hat{h}_l) + \hat{\rho}\hat{U}_a \coth(\hat{k}\hat{h}_a)] + \theta\hat{k}^2[\coth(\hat{k}\hat{h}_l) + \hat{\mu}\coth(\hat{k}\hat{h}_a)]\} \\
&\quad - \hat{k}^2[\hat{U}_l^2 \coth(\hat{k}\hat{h}_l) + \hat{\rho}\hat{U}_a^2 \coth(\hat{k}\hat{h}_a)] + 2i\hat{k}^3\theta[\hat{U}_l \coth(\hat{k}\hat{h}_l) + \hat{\mu}\hat{U}_a \coth(\hat{k}\hat{h}_a)] \\
&\quad + \hat{k}\left[1 + \frac{\hat{\gamma}\hat{k}^2}{(1-\hat{\rho})}\right] = 0.
\end{aligned} \tag{4.1}$$

The expression (2.27) for the neutral curve $\hat{\sigma}_R(\hat{k}) = 0$ is written in dimensionless variables as

$$\hat{V}^2 = \frac{[\tanh(\hat{k}\hat{h}_a) + \hat{\mu}\tanh(\hat{k}\hat{h}_l)]^2}{\tanh(\hat{k}\hat{h}_a) + (\hat{\mu}^2/\hat{\rho})\tanh(\hat{k}\hat{h}_l)} \frac{1}{\hat{k}} \left[1 + \frac{\hat{\gamma}\hat{k}^2}{(1-\hat{\rho})}\right]. \tag{4.2}$$

Notice that the growth rate parameter $\theta = \mu_l/(\rho_l HQ)$, which depends linearly on the kinematic viscosity $\nu_l = \mu_l/\rho_l$ of the liquid, does not appear in (4.2). Note also that the value of $(1 - \hat{\rho})$ is close to unity, since $\hat{\rho} = 0.0012$ for air–water.

The neutral curves for an inviscid fluid (3.5) can be obtained by putting $\hat{\mu} = \hat{\rho}$ or $\mu_l/\rho_l = \mu_a/\rho_a$. This gives from (4.2) the following expression:

$$\hat{V}^2 = [\tanh(\hat{k}\hat{h}_a) + \hat{\rho}\tanh(\hat{k}\hat{h}_l)]\frac{1}{\hat{k}}\left[1 + \frac{\hat{\gamma}\hat{k}^2}{1-\hat{\rho}}\right] \tag{4.3}$$

which is the dimensionless form of (3.6). Though this reduction is immediate it is surprising.

Evaluating (4.2) for $\hat{\mu} = 0$, we get

$$\hat{V}^2 = \tanh(\hat{k}\hat{h}_a)\frac{1}{\hat{k}}\left[1 + \frac{\hat{\gamma}\hat{k}^2}{1-\hat{\rho}}\right]. \tag{4.4}$$

Evaluating (4.2) for $\hat{\mu} = \infty$ we get

$$\hat{V}^2 = \hat{\rho}\tanh(\hat{k}h_l)\frac{1}{\hat{k}}\left[1 + \frac{\hat{\gamma}\hat{k}^2}{1-\hat{\rho}}\right]. \tag{4.5}$$

It is easy to verify that $\hat{V}^2$ is maximum at $\hat{\mu} = \hat{\rho}$, for inviscid fluids. Viscosity in viscous potential flow is destabilizing; however, large viscosities are less destabilizing than small viscosities.

Since $\hat{\rho} = 0.0012$, which is very small, the variation in the stability is large when $\hat{\mu}$ varies between $\hat{\rho}$ and ∞, and is very small when $\hat{\mu}$ varies between $\hat{\rho}$ and zero. The value $\hat{\mu} = 0.018 > \hat{\rho} = 0.0012$, and is in the interval in which $\hat{V}^2$ is rapidly varying (see figure 4).

In the literature on gas–liquid flows a long-wave approximation is often made to obtain stability limits. For long waves $\hat{k} \to 0$ and $\tanh(\hat{k}\hat{h}) \to \hat{k}\hat{h}$ and (4.2) reduces to

$$\hat{V}^2 = \frac{(\hat{h}_a + \hat{\mu}\hat{h}_l)^2}{\hat{h}_a + (\hat{\mu}^2/\hat{\rho})\hat{h}_l}\left[1 + \frac{\hat{\gamma}\hat{k}^2}{1-\hat{\rho}}\right]. \tag{4.6}$$

The effect of surface tension disappears in this limit but the effects of viscosity are important. To obtain the long-wave limit in the inviscid case put $\hat{\mu} = \hat{\rho}$.

The regularization of short waves by surface tension is an important physical effect. For short waves, $\hat{k} \to \infty$, $\tanh(\hat{k}\hat{h}) \to 1$ and

$$\hat{V}^2 = \frac{(\hat{\mu}+1)^2}{1+\hat{\mu}^2/\hat{\rho}}\frac{1}{\hat{k}}\left[1 + \frac{\hat{\gamma}\hat{k}^2}{(1-\hat{\rho})}\right]. \tag{4.7}$$

To obtain the short-wave limit in the inviscid case put $\hat{\mu} = \hat{\rho}$.

The effects of surface tension may be computed from (4.6) and (4.7). The stability limit for long waves $\hat{k} \to 0$ is independent of $\hat{\gamma}$. For short waves (4.6) has a minimum at $\hat{k} = \sqrt{(1-\hat{\rho})/\hat{\gamma}}$ with a value there given by

$$\hat{V}^2 = \frac{2(\hat{\mu}+1)^2}{1+\hat{\mu}^2/\hat{\rho}}\sqrt{\frac{\hat{\gamma}}{1-\hat{\rho}}}. \tag{4.8}$$

Equation (4.8) shows that short waves are stabilized by increasing $\hat{\gamma}$. For small $\hat{\gamma}$ long waves are unstable.

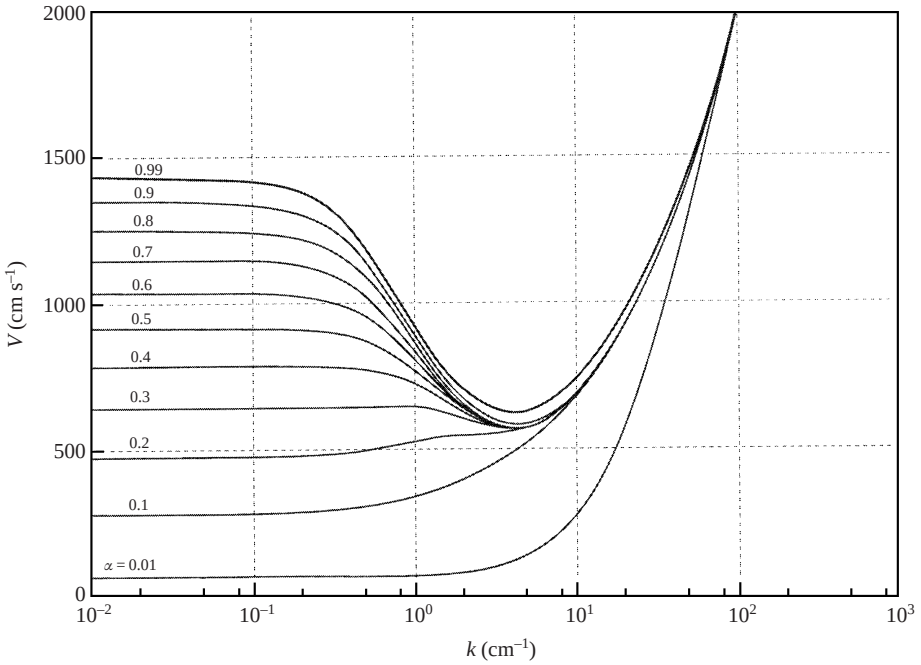

FIGURE 2. Neutral curves for air and water ($\hat{\mu} = 0.018$, see table 1 and figure 4); $\alpha = \hat{h}_a$ is the gas fraction. As in the usual manner, the disturbances will grow above the neutral curve, but decay below it. For α larger than about 0.2, the critical velocity V_c arises, below which all the disturbances will decay.

5. The effect of liquid viscosity and surface tension on growth rates and neutral curves

For air and water at 20 °C

$$\rho_a = 0.0012\,\mathrm{g\,cm^{-3}}, \quad \rho_l = 1\,\mathrm{g\,cm^{-3}}, \quad \hat{\rho} = \rho_a/\rho_l = 0.0012,$$

$$\mu_a = 0.00018\,\mathrm{P}, \qquad \mu_l = 0.01\,\mathrm{P}, \qquad \hat{\mu} = \mu_a/\mu_l = 0.018.$$

The surface tension of air and pure water is $\gamma = 72.8\,\mathrm{dyn\,cm^{-1}}$. Usually the water is slightly contaminated and $\gamma = 60\,\mathrm{dyn\,cm^{-1}}$ is more probable for the water–air tension in experiments. For all kinds of organic liquids $\gamma = 30\,\mathrm{dyn\,cm^{-1}}$ is a good appproximation.

Neutral curves for $\hat{\mu} = 0.018$ (air/water) and $\hat{\mu} = \hat{\rho} = 0.0012$ (inviscid flow) and $\hat{\mu} = 3.6 \times 10^{-6}$ ($\mu_l = 50\,\mathrm{P}$) with $\gamma = 60\,\mathrm{dyn\,cm^{-1}}$ are selected here; the former two are shown in figures 2 and 3. The liquid viscosities $\mu_l = \rho_l\mu_a/\rho_a$ corresponding to these three cases are $\mu_l = 0.01\,\mathrm{P}$, $0.15\,\mathrm{P}$ and $50\,\mathrm{P}$. The neutral curves for $\hat{\mu} \geqslant \hat{\rho}$ are nearly identical. The neutral curves for $\hat{\mu} = 0.018$ (air/water) are to be compared with experiments. We have identified the minimum values of (4.2) over $\hat{k} \geqslant 0$ in the air/water case, and in tables 1, 2 and 3 the critical velocity $V_c = V(k_c)$, the critical wavenumber k_c (and wavelength $\lambda_c = 2\pi/k_c$) and associated wave speeds $\tilde{C}_{Rc} = \tilde{C}_R(k_c)$ are listed. In the tables, V_s and $\tilde{C}_{Rs}$ denote the values taken at $k = 10^{-3}\,\mathrm{cm^{-1}}$, which may be representative of values in the limit of long waves, $k \to 0$. The variation of the critical velocity with the viscosity ratio $\hat{\mu} = \mu_a/\mu_l$ for a representative gas fraction $\alpha = 0.5$ is shown in figure 4. The vertical line $\hat{\mu} = \hat{\rho}$ identifies the stability limit for

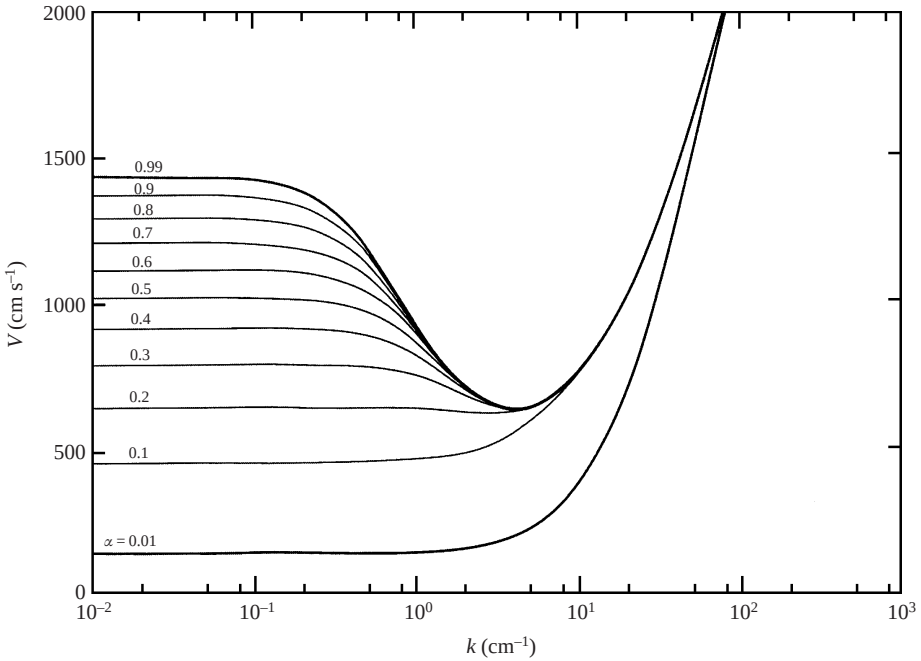

FIGURE 3. Neutral curves for inviscid fluids ($\hat{\mu} = \hat{\rho} = 0.0012$) for different gas fractions $\alpha = \hat{h}_a$. This neutral curve arose for the special case $\hat{\mu} = \hat{\rho} = 0.0012 = \mu_a/\mu_l$ with $\mu_a = 0.00018$ P; hence $\mu_l = 0.15$ P. Surprisingly it is identical to the case $\mu_a = \mu_l = 0$ (see table 2 and figure 4). The neutral curves for viscous fluids with $\mu_l > 15$ cP are essentially the same as these (cf. table 2 and 3).

inviscid fluids. Points to the left of this line have high liquid viscosities $\mu_l > 0.15$ P, and for points to the right, $\mu_l < 0.15$ P.

In all cases the critical velocity is influenced by surface tension; the critical velocity is given by long waves only when α is small (small air gaps). For larger values of α (say $\alpha > 0.2$), the most dangerous neutrally unstable wave is identified by a sharp minimum determined by surface tension, which is identified in table 1 (cf. equation (4.8)).

The growth rates depend strongly on the liquid viscosity, unlike the neutral curves. The most dangerous linear wave is the one whose growth rate σ_R is maximum at $k = k_m$,

$$\sigma_{Rm} = \sigma_R(k_m) = \max_{k \geqslant 0} \sigma_R(k) \tag{5.1}$$

with an associated wavelength $\lambda_m = 2\pi/k_m$ and wave speed $\tilde{C}_{Rm} = \tilde{C}_R(k_m)$. Typical growth rate curves are shown in figure 5. Maximum growth rate parameters for $\hat{\mu} = 0.018$ (figure 5), $\hat{\mu} = \hat{\rho} = 0.0012$, $\mu_l = 15$ cP and $\hat{\mu} = 3.6 \times 10^{-6}$($\mu_l = 50$ P) are listed for $V = 1500$ and 900 cm s^{-1} in table 4.

6. Comparison of theory and experiments in rectangular ducts

Kordyban & Ranov (1970) and Wallis & Dobson (1973) are the only authors to report the results of experiments in rectangular ducts. Many other experiments have been carried out in round pipes; the results of these experiments are not perfectly matched to the analysis done here or elsewhere, and will be discussed later. All

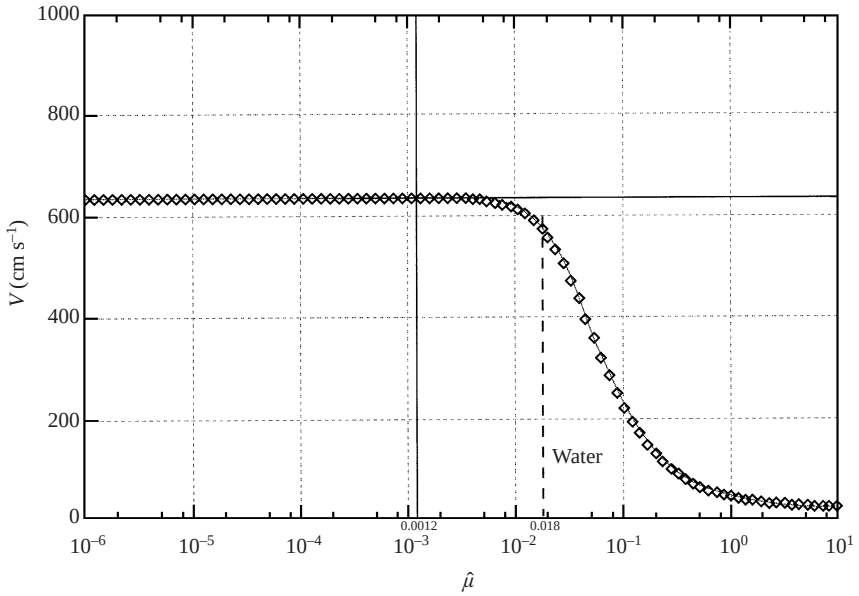

FIGURE 4. Critical velocity V vs. $\hat{\mu}$ for $\alpha = 0.5$. The critical velocity is the minimum value on the neutral curve. The vertical line is $\hat{\mu} = \hat{\rho} = 0.0012$ and the horizontal line at $V = 635.9\,\mathrm{cm\,s^{-1}}$ is the critical value for inviscid fluids. The vertical dashed line at $\hat{\mu} = 0.018$ is for air and water. Typical values for a high-viscosity liquid are given in table 3.

$\hat{h}_a$	$V_s\,(\mathrm{cm\,s^{-1}})$	$\tilde{C}_{Rs}\,(\mathrm{cm\,s^{-1}})$	$k_c\,(\mathrm{cm^{-1}})$	$\lambda_c\,(\mathrm{cm})$	$V_c\,(\mathrm{cm\,s^{-1}})$	$\tilde{C}_{Rc}\,(\mathrm{cm\,s^{-1}})$
0.01	76.04	198.6	0.649	9.676	72.92	155.9
0.1	285.6	43.22				
0.2	478.5	20.82				
0.3	643.4	12.50	0.692	9.076	651.3	9.432
			3.893	1.614	572.5	5.510
0.4	788.8	8.150	4.020	1.563	573.9	5.484
0.5	919.4	5.481	4.052	1.551	574.1	5.481
0.6	1039	3.676	4.052	1.551	574.1	5.479
0.7	1149	2.373	4.052	1.551	574.3	5.459
0.8	1252	1.389	4.117	1.526	575.7	5.319
0.9	1348	0.619	4.354	1.443	585.3	4.415
0.99	1430	0.056	4.150	1.514	628.0	0.585

TABLE 1. Typical values of the neutral curves in figure 2 for air–water with $\rho_a = 0.0012\,\mathrm{g\,cm^{-3}}$, $\mu_a = 0.00018\,\mathrm{P}$, $\rho_l = 1.0\,\mathrm{g\,cm^{-3}}$, $\mu_l = 0.01\,\mathrm{P}$, $g = 980.0\,\mathrm{cm\,s^{-2}}$, $\gamma = 60.0\,\mathrm{dyn\,cm^{-1}}$, $H = 2.54\,\mathrm{cm}$. (This table was based upon the results of computation that the neutral curves with $\alpha = 0.1$ and 0.2 in figure 2 increase monotonically from the values $V_s\,\mathrm{cm\,s^{-1}}$ at $k = 10^{-3}\,\mathrm{cm^{-1}}$; the curve with $\alpha = 0.3$ in figure 2 increases from the value $V_s\,\mathrm{cm\,s^{-1}}$ at $k = 10^{-3}\,\mathrm{cm^{-1}}$, takes a maximum $V = 651.3\,\mathrm{cm\,s^{-1}}$ at $k = 0.692\,\mathrm{cm^{-1}}$, and then takes a minimum $V_c = 572.5\,\mathrm{cm\,s^{-1}}$ (the critical) at $k_c = 3.893\,\mathrm{cm^{-1}}$; for the other values of α, the corresponding curves give the critical V_c at k_c.)

experimenters were motivated to understand the transition from stratified flow with a flat smooth interface to slug flow. They note that in many cases the first transition, which is studied here, is from smooth stratified flow to small-amplitude sinusoidal waves, called capillary waves by Wallis & Dobson (1973). The data given by these authors are framed as a transition to slug flow, though the criteria given are for the

$\hat{h}_a$	V_s (cm s^{-1})	$\tilde{C}_{Rs}$ (cm s^{-1})	k_c (cm^{-1})	λ_c (cm)	V_c (cm s^{-1})	$\tilde{C}_{Rc}$ (cm s^{-1})
0.01	152.2	16.17	0.629	9.990	150.6	9.725
0.1	457.6	4.890				
0.2	645.3	3.082	2.990	2.101	619.8	0.818
0.3	789.5	2.204	3.924	1.601	634.4	0.764
0.4	911.2	1.637	4.020	1.563	635.7	0.762
0.5	1018	1.221	4.052	1.551	635.9	0.762
0.6	1115	0.892	4.052	1.551	635.9	0.762
0.7	1205	0.619	4.052	1.551	635.9	0.759
0.8	1288	0.386	4.052	1.551	635.9	0.738
0.9	1366	0.182	4.052	1.551	635.8	0.590
0.99	1432	0.017	4.052	1.551	635.6	0.078

TABLE 2. Typical values of the neutral curves in figure 3 for air–water (as inviscid fluids) with $\rho_a = 0.0012\,\mathrm{g\,cm^{-3}}$, $\mu_a = 0.0\,\mathrm{P}$, $\rho_l = 1.0\,\mathrm{g\,cm^{-3}}$, $\mu_l = 0.0\,\mathrm{P}$, $g = 980.0\,\mathrm{cm\,s^{-2}}$, $\gamma = 60.0\,\mathrm{dyn\,cm^{-1}}$, $H = 2.54\,\mathrm{cm}$.

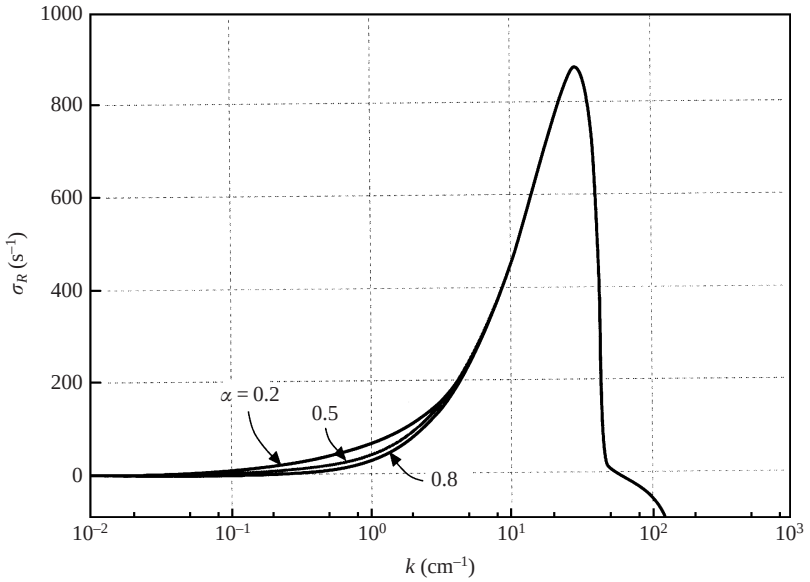

FIGURE 5. The real part of growth rate σ_R s vs. k for $\hat{\mu} = 0.018$ (water, $\mu_l = 1\,\mathrm{cP}$), $V = 1500\,\mathrm{cm\,s^{-1}}$. The graphs are top to bottom $\alpha = 0.2,\ 0.5,\ 0.8$. The curves of $\sigma_R\,\mathrm{s}^{-1}$ along the line of $V = 1500\,\mathrm{cm\,s^{-1}}$ in figure 2, are drawn here for respective values of α. Instability may arise for all the disturbances of wavenumbers below the cut-off wavenumber k_C. The maximum growth rate σ_{Rm} and the corresponding wavenumber $k_m = 2\pi/\lambda_m$ for $V = 1500$ and $900\,\mathrm{cm\,s^{-1}}$ are listed with wave velocity $\tilde{C}_{Rm}$ in table 4.

loss of stability of smooth stratified flow. The theoretical predictions are for the loss of stability, which may or may not be to slug flow.

Note also that all the linear theories that neglect viscosity overpredict the observed stability limit. Wallis & Dobson (1973) note that "... as a result of the present experiments it is our view that the various small wave theories are all inappropriate for describing 'slugging.' Slugging is the result of the rapid development of a large wave which rides over the underlying liquid and can eventually fill the channel to form a slug..." They also note that "It was found possible to produce slugs at

$\hat{h}_a$	V_s (cm s^{-1})	$\tilde{C}_{Rs}$ (cm s^{-1})	k_c (cm^{-1})	λ_c (cm)	V_c (cm s^{-1})	$\tilde{C}_{Rc}$ (cm s^{-1})
0.01	144.0	0.1104				
0.1	455.2	0.0100				
0.2	643.7	0.0045	2.990	2.101	619.4	0.0012
0.3	788.4	0.0026	3.924	1.601	634.1	0.0011
0.4	910.4	0.0017	4.020	1.563	635.4	0.0011
0.5	1018	0.0011	4.052	1.551	635.5	0.0011
0.6	1115	0.0007	4.052	1.551	635.5	0.0011
0.7	1204	0.0005	4.052	1.551	635.5	0.0011
0.8	1287	0.0003	4.052	1.551	635.5	0.0011
0.9	1366	0.0001	4.052	1.551	635.5	0.0009
0.99	1432	1.1×10^{-5}	4.052	1.551	635.5	0.0001

TABLE 3. Typical values of the neutral curves for air–high-viscosity liquid with $\rho_a = 0.0012\,\mathrm{g\,cm^{-3}}$, $\mu_a = 0.00018\,\mathrm{P}$, $\rho_l = 1.0\,\mathrm{g\,cm^{-3}}$, $\mu_l = 50.0\,\mathrm{P}$, $g = 980.0\,\mathrm{cm\,s^{-2}}$, $\gamma = 60.0\,\mathrm{dyn\,cm^{-1}}$, $H = 2.54$ cm; thus $\hat{\mu} = 3.6 \times 10^{-6}$. This corresponds to a high viscosity case in figure 4. (The curves with $\hat{h}_a = 0.5$ through 0.8 take almost the same minimum value at $k = k_c$, though the values at $k = 10^{-3}\,\mathrm{cm^{-1}}$ change as $V_s = 1018$–$1287\,\mathrm{cm\,s^{-1}}$ and $\tilde{C}_{Rs} = 0.0011$–$0.0003\,\mathrm{cm\,s^{-1}}$). (See table 4 for the maximum growth rate.)

air fluxes less than those predicted" by their empirical formula, $j^* < 0.5\alpha^{3/2}$. All this suggests that we may be looking at something akin to subcritical bifurcation with multiple solutions and hysteresis.

Turning next to linearized theory Wallis & Dobson (1973) do an inviscid analysis and state that "... if waves are 'long' ($kh_L \ll 1$, $kh_G \ll 1$) and surface tension can be neglected, the predicted instability condition is

$$(v_G - v_L)^2 > (\rho_L - \rho_G)\, g \left(\frac{h_G}{\rho_G} + \frac{h_L}{\rho_L} \right). \tag{6.1}$$

If $\rho_G \ll \rho_L$ and $v_L \ll v_G$ they may be simplified further to give

$$\rho_G v_G^2 > g(\rho_L - \rho_G) h_G \tag{6.2}$$

which is the same as

$$j_G^* > \alpha^{3/2} \tag{6.3}$$

... " Here $\alpha = h_G/H$ and

$$j_G^* = \frac{v_G \alpha \sqrt{\rho_G}}{\sqrt{gH(\rho_L - \rho_G)}} > \alpha^{3/2}.$$

Their criterion (6.1) is identical to our (4.6) for the long-wave inviscid case $\hat{\mu} = \hat{\rho}$ and $\hat{k} \to 0$. They compare their criterion (6.3) with transition observations that they call 'slugging' and note that empirically the stability limit is described well by

$$j_G^* > 0.5\alpha^{3/2},$$

rather than (6.3).

In figure 6 we plot j^* vs. α showing $j_G^* = \alpha^{3/2}$ and $0.5\alpha^{3/2}$; we give the results from our viscous potential flow theory for the inviscid case in table 2 and the air–water case in table 1 and we show the experimental results presented by Wallis & Dobson (1973) and Kordyban & Ranov (1970). Our theory fits the data better than Wallis &

$\hat{\mu}$	V (cm s^{-1})	$\hat{h}_a$	k_m (cm^{-1})	λ_m (cm)	σ_{Rm} (s^{-1})	$\tilde{C}_{Rm}$ (cm s^{-1})
0.018	1500	0.01	29.90	0.2101	1448	3.044
		0.1–0.9	29.66	0.2118	872.5	2.049
		0.99	32.13	0.1955	706.2	1.454
	900	0.01	15.40	0.408	615.3	3.046
		0.1	10.00	0.628	167.7	1.183
		0.2	10.24	0.613	164.2	1.175
		0.3–0.8	10.24	0.613	164.2	1.174
		0.9	10.33	0.609	163.3	1.164
		0.99	11.36	0.553	84.66	0.367
0.0012	1500	0.01	26.95	0.233	1340	3.022
		0.1–0.9	27.17	0.231	768	1.798
		0.99	30.14	0.209	584.7	1.159
	900	0.01	14.45	0.435	585.2	3.064
		0.1	9.456	0.665	155.1	1.097
		0.2–0.7	9.685	0.649	151.0	1.079
		0.8	9.763	0.644	151.0	1.079
		0.9	9.841	0.638	149.9	1.064
		0.99	10.66	0.589	69.59	0.285
3.6×10^{-6}	1500	0.01	1.821	3.450	295.1	24.55
		0.1	0.916	6.861	60.04	4.495
		0.2	0.845	7.432	34.43	2.049
		0.3	3.087	2.035	21.96	0.086
		0.4–0.6	4.4–4.5	1.42–1.40	21.89	0.045–0.04
		0.7	4.679	1.343	21.85	0.040
		0.8	5.360	1.172	21.61	0.032
		0.9	7.743	0.812	20.21	0.017
		0.99	20.54	0.306	6.801	0.003
	900	0.01	1.323	4.750	145.9	19.64
		0.1	0.676	9.297	24.80	3.017
		0.2	0.581	10.82	10.48	1.199
		0.3	0.984	6.385	4.294	0.135
		0.4–0.6	4.02–4.08	1.56–1.51	4.86	0.010
		0.7	4.150	1.514	4.840	0.009
		0.8	4.460	1.409	4.735	0.008
		0.9	5.534	1.135	4.100	0.005
		0.99	7.994	0.786	0.741	0.001

TABLE 4. Wavenumber, wavelength and wave speed for the maximum growth rate (5.1).

Dobson's (1973) $j^* = \alpha^{3/2}$ curve; it still overpredicts the data for small α but fits the large α data quite well; we have good agreement when the water layer is small.

The predicted wavelength and wave speed in table 1 can be compared with experiments in principle, but in practice this comparison is obscured by the focus on the formation of slugs. For example, Wallis & Dobson (1973) remark that "at a certain minimum air velocity, ripples appeared at the air entry end, and slowly spread down the channel. These waves were about 2-in. (0.05 m) long and were made up of long wave crests, with three or four capillary waves riding on the troughs. The long waves traveled faster than the capillary waves." The speed of these long waves was reported by Wallis & Dobson (1973) to be less than 0.3 m s^{-1} in all cases. Theoretical results from table 1 show that the wavelength λ_c increases with the water depth (as in

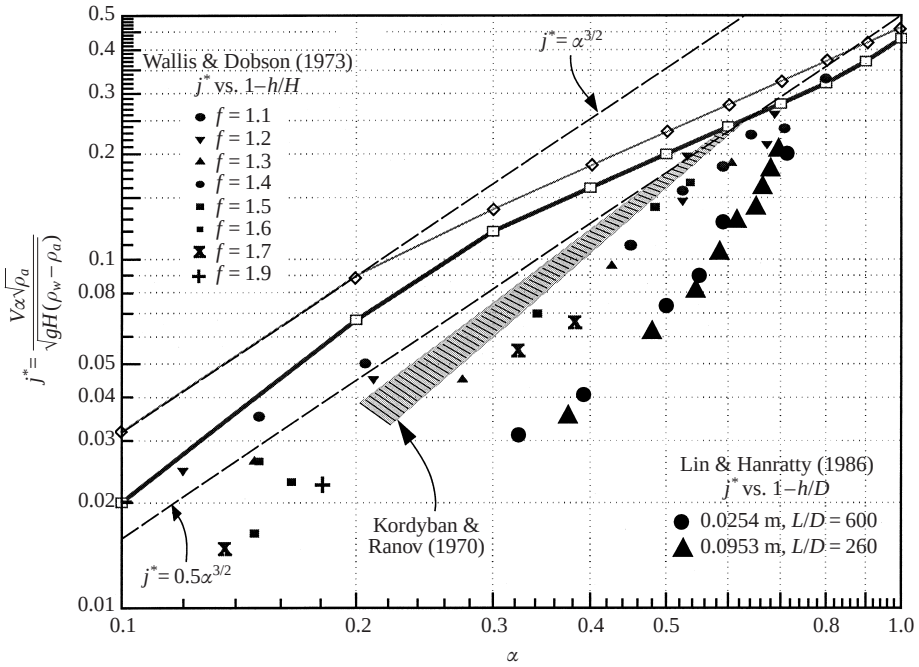

FIGURE 6. j^* vs. α is for marginal stability of air and water in a frame in which the water velocity is zero. The heavy line through $\square$ = air–water, our result with $\gamma = 60$ dynes/cm from table 1; $\diamond$ = inviscid fluid from table 2. $j^* = \alpha^{3/2}$ is the long-wave criterion for an inviscid fluid put forward by Wallis & Dobson (1973). $j^* = 0.5\alpha^{3/2}$ was proposed by them as best fit to the experiments $f1.1$ through $f1.9$ described in their paper. The shaded region is from experiments by Kordyban & Ranov (1970). Also shown are experimental data in rectangular conduits j^* vs. $1 - h/H = \alpha$ and in round pipes j^* vs. $1 - h/D = \alpha$ (Lin & Hanratty 1986, figure 4).

the experiment) and the wave speed varies from $0.1\,\mathrm{m\,s^{-1}}$ to $0.04\,\mathrm{m\,s^{-1}}$. The predicted spacing of the waves on average is about $1.5\,\mathrm{cm\,s^{-1}}$. The predicted wavelength and wave speed from viscous potential flow are apparently in good agreement with the waves Wallis & Dobson (1973) call capillary waves.

Observations similar to those of Wallis & Dobson (1973) were made by Andritsos, Williams & Hanratty (1989) who note that for high-viscosity liquid (80 cP) a region of regular two-dimensional waves barely exists. "The first disturbances observed with increasing gas velocity are small-amplitude, small-wavelength, rather regular 2D waves. With a slight increase in gas velocity, these give way to a few large-amplitude waves with steep fronts and smooth troughs, and with spacing that can vary from a few centimeters to a meter."

7. Critical viscosity and density ratios

The most interesting aspect of our potential flow analysis is the surprising importance of the viscosity ratio $\hat{\mu} = \mu_a/\mu_l$ and density ratio $\hat{\rho} = \rho_a/\rho_l$; when $\hat{\mu} = \hat{\rho}$ equation (4.2) for marginal stability is identical to the equation for the neutral stability of an inviscid fluid even though $\hat{\mu} = \hat{\rho}$ in no way implies that the fluids are inviscid. Moreover, the critical velocity is a maximum at $\hat{\mu} = \hat{\rho}$; hence the critical velocity is smaller for all viscous fluids such that $\hat{\mu} \neq \hat{\rho}$ and is smaller than the critical velocity for inviscid fluids. All this may be understood by inspection of figure 4, which shows

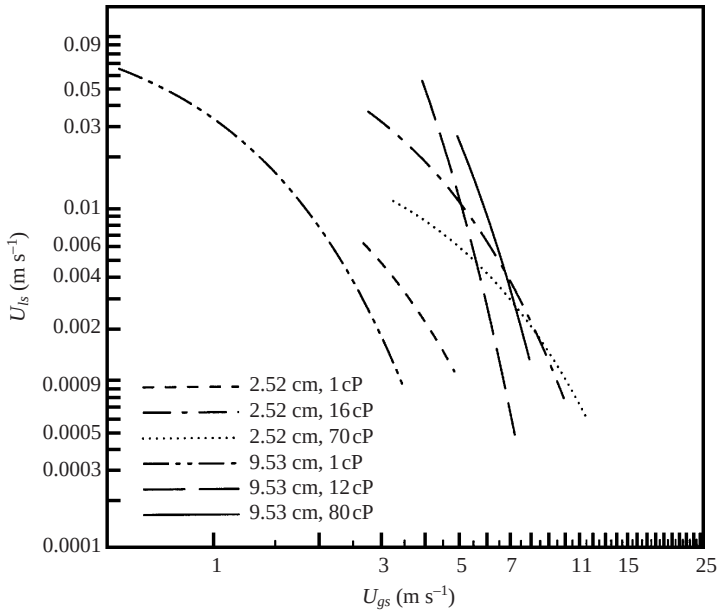

FIGURE 7. (After Andritsos & Hanratty 1987.) The borders between smooth stratified flow and disturbed flow observed in experiment for various heights of the liquid and viscosities. The water–air data are well below the cluster of high-viscosity data that are bunched together.

that $\hat{\mu} = \hat{\rho}$ is a distinguished value that can be said to divide high-viscosity liquids with $\hat{\mu} < \hat{\rho}$ from low-viscosity liquids. The stability limits of high-viscosity liquids can hardly be distinguished from each other while the critical velocity decreases sharply for low-viscosity fluids. This result may be framed in terms of the kinematic viscosity $v = \mu/\rho$ with high viscosities $v_l > v_a$. The condition $v_a = v_l$ can be written as

$$\mu_l = \mu_a \frac{\rho_l}{\rho_a}. \tag{7.1}$$

For air and water

$$\mu_l = 0.15 \text{ P}. \tag{7.2}$$

Hence $\mu_l > 0.15$ P is a high-viscosity liquid and $\mu_l < 0.15$ P is a low-viscosity liquid provided that $\rho_l \approx 1 \text{ g cm}^{-3}$.

Other authors have noted unusual relations between viscous and inviscid fluids. Barnea & Taitel (1993) note that "the neutral stability lines obtained from the viscous Kelvin-Helmholtz analysis and the inviscid analysis are quite different for the case of low liquid viscosities, whereas they are quite similar for high viscosity, contrary to what one would expect." Their analysis starts from a two-fluid model and it leads to different dispersion relations; they do not obtain the critical condition $\hat{\mu} = \hat{\rho}$. Earlier, Andritsos *et al.* (1989) noted a "surprising result that the inviscid theory becomes more accurate as the liquid viscosity increases."

Andritsos & Hanratty (1987) have presented flow regime maps for flows in 2.52 cm and 9.53 cm pipes for fluids of different viscosity ranging from 1 cP to 80 cP. These figures present flow boundaries; the boundaries of interest to us are those that separate 'smooth' flow from disturbed flow. Liquid holdups (essentially α) are not specified in these experiments. We extracted the smooth flow boundaries from figures in Andritsos & Hanratty (1987) and collected them in our figure 7. It appears from this figure that

the boundaries of smooth flow for all the liquids with $\mu_l > 15\,\text{cP}$ are close together, but the boundary for water with $\mu_l = 1\,\text{cP}$ is much lower. The velocities shown in these figures are superficial velocities; the average velocities which could be compared with critical velocities in tables 1, 2 and 3 are larger than the superficial velocities and are significantly larger than those in the tables.

Even earlier Francis (1951) had observed that though the inviscid prediction of the KH instability overestimates the onset for air over water, this prediction is in good agreement with experiments in rectangular ducts when air is above water.

8. Further comparisons with previous results

In practice, interest in the pipelining of gas–liquid flow is in round pipes. All experiments other than those of Kordyban & Ranov (1970) and Wallis & Dobson (1973) reviewed in § 6 have been carried out in round pipes. To our knowledge there is no other theoretical study in which the stability of stratified flow in a round pipe is studied without approximations. Theoretical studies of stability of stratified flow have been presented by Wallis (1969), Wu *et al.* (1987), Barnea (1991), Crowley, Wallis & Barry (1992), Kordyban & Ranov (1970), Wallis & Dobson (1973), Taitel & Dukler (1976), Mishima & Ishii (1980), Lin & Hanratty (1986), Andritsos & Hanratty (1987), Andritsos *et al.* (1989), Barnea & Taitel (1993). Viscosity is neglected by Kordyban & Ranov (1970), Wallis & Dobson (1973), Taitel & Dukler (1976) and Mishima & Ishii (1980). Surface tension is neglected by Wallis (1969), Kordyban & Ranov (1970), Wallis & Dobson (1973), Taitel & Dukler (1976), Mishima & Ishii (1980) and Lin & Hanratty (1986). Wallis (1969), Lin & Hanratty (1986), Wu *et al.* (1987), Barnea (1991), Crowley *et al.* (1992) and Barnea & Taitel (1993) use one or other of the forms of two-fluids equations. In these equations averaged variables are introduced, the actual geometry is represented only so far as its area and round, elliptical or rectangular pipes with equal areas are equivalent. The effects of viscosity in these averaged models are introduced through empirical wall and interfacial fraction correlations. All these authors neglect the normal component of viscous stress (extensional stresses are neglected). The approach of Andritsos & Hanratty (1987), Andritsos *et al.* (1989) is different: all the main physical effects are represented in an analysis of the plane flow which is later applied to flow in round pipes. The disturbance equations for the liquid are solved exactly except that the shear of the basic liquid flow is neglected using a plug flow assumption. The effects of the gas on the liquid are represented through empirical correlations and further approximations are required for round pipes.

The viscous analysis of Andritsos & Hanratty (1987) for stability of stratified flow indicates that the critical velocity increases with increasing viscosity unlike the present analysis which predicts no such increase when $v_l > v_a$. The discrepancy may be due to the approximations made by Andritsos & Hanratty (1987).

Experiments on the stability of stratified flow have been reported by Kordyban & Ranov (1970), Wallis & Dobson (1973), Taitel & Dukler (1976), Lin & Hanratty (1986), Crowley *et al.* (1992) and Andritsos & Hanratty (1987). The experiments of Lin & Hanratty (1986) and Andritsos & Hanratty (1987) do not have data giving the height of the liquid and gas layers. Kordyban & Ranov (1970) and Wallis & Dobson (1973) did experiments in rectangular ducts, the geometry analysed in this paper, the other experiments were done in round pipes. Lin & Hanratty (1986), Crowley *et al.* (1992) and Andritsos & Hanratty (1987) are the only experimenters to report results for fluids with different viscosities.

It is difficult to compare the results of experiments in round pipes and rectangular

channels. The common practice for round pipes is to express results in terms of h/D where D is the pipe diameter and h is the height of liquid above the bottom of the pipe; h/H is the liquid fraction in rectangular pipes and $\alpha = 1 - h/H$ is the gas fraction, but h/D is not the liquid fraction in round pipes and $1 - h/D$ is not the gas fraction in round pipes. Lin & Hanratty (1986) presented experimental results for thin liquid films in round pipes giving (their figure 4) h/D vs. j^*; we converted their results to j^* vs. $1 - h/D$ and compared them in figure 6 with the results for rectangular pipes. The experimental results for round pipes are much lower than those for rectangular pipes. All this points to the necessity of taking care when comparing results between round and rectangular pipes and interpreting results of analysis for one experiment to another.

In general we do not expect viscous potential flow analysis to work well in two-liquid problems; we get good results only when one of the fluids is a gas so that retarding effects of the second liquid can be neglected. However, the case of Holmboe waves studied by Pouliquen, Chomaz & Huerre (1994) may have a bearing on the two-liquid case. These waves appear only near our critical condition of equal kinematic viscosity. They account for viscosity by replacing the vortex sheet with layers of constant vorticity across which no-slip conditions and the continuity of shear stress are enforced for the basic flow but the disturbance is inviscid. They did not consider the notion that an inviscid analysis is just what would emerge from the condition of equal kinematic viscosity for viscous potential flow.

9. Nonlinear effects

None of the theories agree with experiments. Attempts to represent the effects of viscosity are only partial, as in our theory of viscous potential flow, or they require empirical data on wall and interfacial friction, which are not known exactly and may be adjusted to fit the data. Some choices for empirical inputs underpredict and others overpredict the experimental data.

It is widely acknowledged that nonlinear effects at play in the transition from stratified to slug flow are not well understood. The well-known criterion of Taitel & Dukler (1976), based on a heuristic adjustment of the linear inviscid long-wave theory for nonlinear effects, is possibly the most accurate predictor of experiments. Their criterion replaces $j^* = \alpha^{3/2}$ with $j^* = \alpha^{5/2}$. We can obtain the same heuristic adjustment for nonlinear effects on viscous potential flow by multiplying the critical value of the velocity in table 1 by α. Plots of $j^* = \alpha^{3/2}$, $j^* = \alpha^{5/2}$ and the heuristic adjustment of viscous potential flow, together with the experimental values of Wallis & Dobson (1973) and Kordyban & Ranov (1970) are shown in figure 8. The good agreement there lacks a convincing foundation.

10. Conclusion

We studied Kelvin–Helmholtz stability of superposed uniform streams in rectangular ducts using viscous potential flow analysis. Viscous potential flows satisfy the Navier–Stokes equations. Because the no-slip condition cannot be satisfied the effects of shear stresses are neglected, but the effects of extensional stresses at the interface on the normal stresses are fully represented. The solution presented is complete and mathematically rigorous. The effects of shear stresses are neglected at the outset; after that no empirical inputs are introduced. The main result of the analysis is the emergence of a critical value of velocity, discussed in § 7. The main consequence of

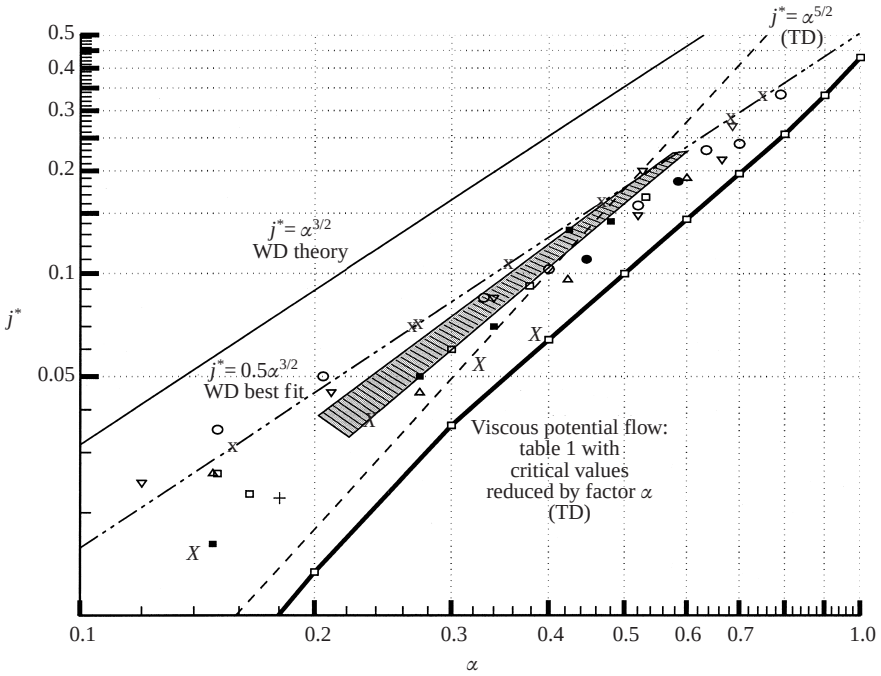

FIGURE 8. Nonlinear effects. The Taitel–Dukler (1976) (TD) correction (multiply by α). WD denotes Wallis & Dobson (1973).

this result is that for air–liquid systems the critical values of velocity for liquids with viscosities greater than 15 cP are essentially independent of viscosity and the same as for an inviscid fluid, but for liquids with viscosities less than 15 cP the stability limits are much lower. The criterion for stability of stratified flow given by viscous potential flow analysis is in good agreement with experiments when the liquid layer is thin, but it overpredicts the data when the liquid layer is thick. Though viscous potential flow neglects the effects of shear the qualitative prediction of the unusual effects of liquid viscosity have been obtained by other authors using other methods of analysis in which shear is not neglected.

A quite accurate predictor of experimental results is given by applying the nonlinear correction factor to account for the effect of finite-amplitude waves on the results of viscous potential flow.

This work was supported by the Engineering Research Program of the Office of Basic Energy Sciences at the DOE, by the NSF/CTS-0076648, by an ARO grant DA/DAAH04 and by INTEVEP S.A. A longer (unreferred) version of this paper can be found at http://www.aem.umn.edu/people/faculty/joseph/.

REFERENCES

ANDRITSOS, N. & HANRATTY, T. J. 1987 Interfacial instabilities for horizontal gas-liquid flows in pipelines. *Intl J. Multiphase Flow* **13**, 583–603.

ANDRITSOS, N., WILLIAMS, L. & HANRATTY, T. J. 1989 Effect of liquid viscosity on the stratified-slug transition in horizontal pipe flow. *Intl J. Multiphase Flow* **15**, 877–892.

BARNEA, D. 1991 On the effect of viscosity on stability of stratified gas-liquid flow – application to flow pattern transition at various pipe inclinations. *Chem. Engng Sci.* **46**, 2123–2131.

Barnea, D. & Taitel, Y. 1993 Kelvin-Helmholtz stability criteria for stratified flow: viscous versus non-viscous (inviscid) approaches. *Intl J. Multiphase Flow* **19**, 639–649.

Charru, F. & Hinch, E. J. 2000 'Phase diagram' of interfacial instabilities in a two-layer Couette flow and mechanism of the long-wave instability. *J. Fluid Mech.* **414**, 195–224.

Crowley, C. J., Wallis, G. B. & Barry, J. J. 1992 Validation of a one-dimensional wave model for the stratified-to-slug flow regime transition, with consequences for wave growth and slug frequency. *Intl J. Multiphase Flow* **18**, 249–271.

Francis, J. R. D. 1951 The aerodynamic drag of a free water surface. *Proc. R. Soc. Lond.* A **206**, 387–406.

Joseph, D. D., Belanger, J. & Beavers, G. S. 1999 Breakup of a liquid drop suddenly exposed to a high-speed airstream. *Intl J. Multiphase Flow* **25**, 1263–1303.

Joseph, D. D. & Liao, T. 1994 Potential flows of viscous and viscoelastic fluids. *J. Fluid Mech.* **265**, 1–23.

Joseph, D. D. & Renardy, Y. Y. 1991 *Fundamentals of Two-Fluid Dynamics*, Chap. IV–VIII, Springer.

Joseph, D. D. & Saut, J.-C. 1990 Short wave instabilities and ill-posed problems. *Theor. Comput. Fluid Mech.* **1**(4), 191–228.

Kordyban, E. S. & Ranov, T. 1970 Mechanism of slug formation in horizontal two-phase flow. *Trans. ASME: J. Basic Engng* **92**, 857–864.

Lin, P. Y. & Hanratty, T. J. 1986 Prediction of the initiation of slugs with linear stability theory. *Intl J. Multiphase Flow* **12**, 79–98.

Mishima, K. & Ishii, M. 1980 Theoretical prediction of onset of horizontal slug flow. *Trans. ASME: J. Fluids Engng* **102**, 441–445.

Pouliquen, O., Chomaz, J. M. & Huerre, P. 1994 Propagating Holmboe waves at the interface between two immiscible fluids. *J. Fluid Mech.* **226**, 277–302.

Taitel, Y. & Dukler, A. E. 1976 A model for predicting flow regime transitions in horizontal and near horizontal gas-liquid flow. *AIChE J.* **22**, 47–55.

Wallis, G. B. 1969 *One-dimensional Two-phase Flow*. McGraw-Hill.

Wallis, G. B. & Dobson, J. E. 1973 The onset of slugging in horizontal stratified air-water flow. *Intl J. Multiphase Flow* **1**, 173–193.

Wu, H. L., Pots, B. F. M., Hollenberg, J. F. & Meerhoff, R. 1987 Flow pattern transitions in two-phase gas/condensate flow at high pressure in an 8-inch horizontal pipe. *Third Intl Conf. on Multiphase Flow, The Hague, The Netherlands*, Paper A2, pp. 13–21.